Selection and Characterization of Artificial Proteins Targeting the Tubulin α Subunit

Valérie Campanacci, Agathe Urvoas, Tanja Consolati, Soraya Cantos-Fernandes, Magali Aumont-Nicaise, Marie Valerio-Lepiniec, Thomas Surrey, Philippe Minard, Benoît Gigant

Selection and characterization of artificial proteins targeting the tubulin α subunit

Valérie Campanacci[1,4], Agathe Urvoas[1,4], Tanja Consolati[2], Soraya Cantos-Fernandes[1], Magali Aumont-Nicaise[1], Marie Valerio-Lepiniec[1], Thomas Surrey[2], Philippe Minard[1,*] & Benoît Gigant[1,3,*]

[1] Institute for Integrative Biology of the Cell (I2BC), CEA, CNRS, Univ. Paris-Sud, Université Paris-Saclay, 91198, Gif-sur-Yvette cedex, France

[2] The Francis Crick Institute, 1 Midland Road, London NW1 1AT, UK

[3] Lead contact

[*] Correspondence: philippe.minard@i2bc.paris-saclay.fr (P.M.), benoit.gigant@i2bc.paris-saclay.fr (B.G.).

[4] These authors contributed equally

Summary

Microtubules are cytoskeletal filaments of eukaryotic cells made of αβ-tubulin heterodimers. Structural studies of non-microtubular tubulin rely mainly on molecules that prevent its self-assembly and are used as crystallization chaperones. Here we identified artificial proteins from an αRep library that are specific to α-tubulin. Turbidity experiments indicate that these αReps impede microtubule assembly in a dose-dependent manner and total internal reflection fluorescence microscopy further shows that they specifically block growth at the microtubule (-) end. Structural data indicate that they do so by targeting the α-tubulin longitudinal surface. Interestingly, in one of the complexes studied, the α subunit is in a conformation that is intermediate between the ones most commonly observed in X-ray structures of tubulin and those seen in the microtubule, emphasizing the plasticity of tubulin. These α-tubulin-specific αReps broaden the range of tools available for the mechanistic study of microtubule dynamics and its regulation.

Introduction

Microtubules are eukaryotic cytoskeletal assemblies involved in critical functions ranging from intracellular trafficking to ciliogenesis and cell division. To achieve these different functions, cells constantly reorganize their microtubule network, regulating microtubule nucleation and dynamics. Microtubules are hollow tubes made of parallel protofilaments formed by the head-to-tail assembly of αβ-tubulin heterodimers (tubulin). As a result, microtubules are polar structures, with a (-) end where α-tubulin subunits are exposed, and a faster growing (+) end, terminated by β-tubulin subunits (Desai and Mitchison, 1997). Our understanding of microtubule dynamics and of its regulation is still incomplete, in particular from a structural point of view, although continuous progress has been made over the past two decades. Indeed, microtubule structures are now available at near 3 Å resolution from cryo-electron microscopy data (Benoit et al., 2018; Howes et al., 2017; Zhang et al., 2015; Zhang et al., 2018). In addition, crystal structures of non-microtubular tubulin have been obtained despite the notorious difficulty to crystallize this protein, which is related to its propensity to self-assemble into heterogeneous species. Two general strategies have been pursued to circumvent this limitation. In one of them, mutations that diminish longitudinal contacts between tubulin molecules have been introduced to disfavor self-assembly (Johnson et al., 2011). This tubulin mutant has been crystallized in complex with TOG domain proteins (Ayaz et al., 2014; Ayaz et al., 2012). The second approach is based on proteins that make well-defined complexes with tubulin, unable to assemble further. These proteins are either vertebrate stathmin-like domain proteins (SLDs) that form with tubulin a 2:1 tubulin:SLD assembly (T_2SLD) (Jourdain et al., 1997) or artificial Designed Ankyrin Repeat Proteins (DARPins) (Plückthun, 2015) selected to bind β-tubulin (Pecqueur et al., 2012), and high resolution crystal structures of tubulin have been obtained with SLDs or with DARPins used as crystallization chaperones (Ahmad et al., 2016; Mignot et al., 2012; Nawrotek et al., 2011)}. These proteins have also proven useful to study the mechanism of microtubule-associated proteins (MAPs) that interact with tubulin, both structurally (Cao et al., 2014; Gigant et al., 2013; Prota et al., 2013b; Wang et al., 2017) and biochemically (Gigant et al., 2014; Li et al., 2015). However, both SLDs and DARPins may compete with MAPs for tubulin binding. Indeed, SLDs target a tubulin surface that corresponds to the exterior of the microtubule (Gigant et al., 2000), where the binding sites of numerous MAPs are clustered (Nogales and Kellogg, 2017). Competition with DARPins has also been reported (Nawrotek et al., 2014; Sharma et al., 2016). Therefore, there is a need to expand the tools available to study microtubules with proteins that bind tubulin differently from SLDs or from the DARPins used so far. In particular, only a few molecules that stabilize tubulin without interacting with its β subunit have been described (e.g., (Clément et al., 2005; Wang et al., 2012)).

We present here the selection and characterization of αReps that target the tubulin α subunit. αReps are artificial proteins based on a consensus sequence of a HEAT-like repeated motif initially observed in thermophilic microorganisms (Guellouz et al., 2013; Urvoas et al., 2010). We show that selected αReps prevent microtubule assembly with a specific blocking effect at the (-) end, and we have determined their structure in complex with tubulin to rationalize this inhibition. These tubulin-binding αReps broaden the range of tools available to study tubulin, in particular its regulation by β-tubulin-specific proteins.

Results and discussion.

Selection of α-tubulin-specific αReps.

The in vitro selection of binders from a library of artificial proteins is usually performed on an immobilized target. In the case of a protein target, to preserve its native structure, this step often takes advantage of tags, e.g. a biotinylated tag that interacts with immobilized streptavidin (Guellouz et al., 2013). However, whereas systems to express recombinant tubulin are now available (Johnson et al., 2011; Minoura et al., 2013; Ti et al., 2016; Vemu et al., 2016), purification of this protein from natural sources is still the most efficient way to obtain the large quantities needed for biochemical experiments. We therefore decided to use for selection the same protein, purified from sheep brain, that will be used in later experiments. To bias the selection towards α-tubulin binders, we immobilized a β-tubulin-specific biotinylated DARPin on a streptavidin-coated plate (Fig. 1A). In addition, to increase the residence time of tubulin on the plate, we used a high affinity, slowly dissociating DARPin (Ahmad et al., 2016). An αRep library (Guellouz et al., 2013) was then screened through 3 rounds of phage display, and αReps that bind tubulin were identified in an ELISA assay. Two αReps, named iE5 and iiH5, which were among those giving the highest signal in this assay, and which comprise 5 and 3 internal repeats, respectively, were chosen for further biochemical and structural characterization.

The iE5 and iiH5 αReps bind tubulin and inhibit microtubule assembly.

In the ELISA assay, the interaction of the αReps with tubulin was monitored while the latter was immobilized (Fig. 1A). To ascertain the interaction in solution, we performed size exclusion chromatography experiments (Fig. 1B). Compared to tubulin alone, a chromatographic peak that eluted earlier was observed when tubulin:αRep samples were loaded on the column. SDS-PAGE analysis of the protein content of that peak indicated the presence of both tubulin and either of the αReps (Fig. 1C). These results confirm that both iE5 and iiH5 form a complex with tubulin. In addition, because the injected samples were prepared with a slight molar excess of αRep, and because a peak corresponding to free αReps (not bound to tubulin) was detected (Fig. 1B), the size exclusion chromatography experiments suggest that the stoichiometry of binding is one tubulin molecule for one αRep in both cases.

The gel filtration profile is characteristic of a tight interaction. For both αReps, the peak of the complex was nearly symmetrical, and the tubulin peak was completely displaced. To characterize the strength of the association of tubulin with iE5 and iiH5 further, we studied the tubulin:αRep interaction by isothermal titration calorimetry (ITC). The titration of tubulin by iE5 led to a dissociation constant (K_D) of 270 ± 75 nM whereas the same experiment with iiH5 led to a K_D of 95 ± 15 nM (Fig. 1D,E; Table 1). These values are within the range usually found between selected αReps and their target protein (Chevrel et al., 2018; Guellouz et al., 2013) and correspond to reasonably tight interactions.

Then we recorded the effect of iE5 and iiH5 on microtubule assembly using a turbidity assay. We found that the turbidity signal corresponding to microtubule assembly decreased in presence of both αReps (Fig. 1F,G). These experiments further supported the 1:1 tubulin:αRep binding stoichiometry, in agreement with the gel filtration analysis (Fig. 1B) and the ITC data (Table 1). For instance, the turbidity plots of 20 µM tubulin in

presence of 5 µM iE5 (Fig. 1F) or iiH5 (Fig. 1G) are similar to the ones of the 15 µM tubulin control. The same applies when comparing a 10 µM tubulin solution and samples consisting of 20 µM tubulin and 10 µM αRep. Finally, when a stoichiometric amount of αRep was added to 20 µM tubulin, almost no turbidity signal was detected. Taken together, these results show that both αReps inhibit microtubule assembly in a dose-dependent manner. To elucidate the basis of this mechanism, we determined the structure of the corresponding tubulin–αRep complexes.

iE5 and iiH5 target the longitudinal surface of α-tubulin.

The X-ray structure of tubulin–iE5 was determined by molecular replacement at a resolution of 2.6 Å (Table 2). The structure confirmed the 1:1 tubulin:iE5 stoichiometry (Fig. 2A) and there was one complex per asymmetric unit. In agreement with the selection strategy (Fig. 1A), the αRep binds to α-tubulin. It targets a mostly acidic surface (Fig. 2B) that is involved in tubulin–tubulin longitudinal contacts within microtubules (Nogales et al., 1999) (Fig. 2C). It interacts in particular with the α-tubulin T7 loop and the following H8 helix, and with the H10-S9 loop and the S9 β-strand (Fig. 2A,D) (see (Löwe et al., 2001) and Fig. S1 for tubulin secondary structure nomenclature and domain definition). On the αRep side, the binding surface is electropositive (Fig. 2D) and formed by many residues from randomized positions but also by some (invariant) residues of the framework (Fig. 2E), as commonly observed in αRep selection (Guellouz et al., 2013).

The structure of tubulin–iiH5 was similarly determined to 3.2 Å resolution (Table 2, Fig. 3A). There are 3, virtually identical, complexes in the asymmetric unit (pairwise root mean square deviations (r.m.s.d.) ranging from 0.39 to 0.50 Å; about 1010 Cαs compared). In the crystal, tubulin–iiH5 formed a helical structure with 6 complexes per turn and a pitch of 54 Å, i.e. the width of one tubulin (Fig. 3B). Several features of the tubulin–iE5 structure also apply to tubulin–iiH5. Indeed, iiH5 makes a 1:1 assembly with tubulin. It binds to the (acidic) longitudinal surface of the α subunit (Fig. 3C). It interacts in particular with the T7 and the S8-H10 loops and with the S9 strand (Fig. 3A,D). iiH5 also interacts with the N-terminal H1-S2 loop. In addition, the iiH5 binding surface is basic (Fig. 3D) and is mostly formed by residues at randomized positions (Fig. 3E). The binding to the longitudinal surface of α-tubulin, which is exposed at the microtubule (-) end (Fig. S2), suggests that these αReps may affect the two ends of the microtubule differently.

iE5, iiH5 and a tandem repeat αRep stop growth at the microtubule (-) end.

To discriminate between effects the αReps have on the growth of the two different microtubule ends, we imaged individual microtubules using a total internal reflection fluorescence microscopy (TIRFM) assay (Roostalu et al., 2015), in which dynamic microtubules grew in the presence of 15 µM tubulin from immobilized GMPCPP-microtubule 'seeds'. In the absence of αReps, microtubule (+) and (-) ends elongated with speeds of ~ 20 nm s^{-1} and 4 nm s^{-1}, respectively (Fig. 4). The addition of 1 µM of iE5 (Fig. 4C,H) or of iiH5 (Fig. 4E,I) substantially reduced the (-) end growth speed, whereas the (+) end growth speed was unaffected. To test if this selective inhibitory effect of (-) end growth can be increased, we constructed a tandem repeat version of the iiH5 αRep (Fig. S2), termed $(iiH5)_2$, as it was done previously with a β-tubulin targeting DARPin (Pecqueur et al., 2012). We first verified using a turbidity assay that the inhibition of

microtubule assembly by $(iiH5)_2$ (Fig. 1H) agrees with the formation of a 2:1 tubulin:$(iiH5)_2$ complex (Campanacci et al, submitted). TIRFM experiments then demonstrated that $(iiH5)_2$ indeed inhibited (-) end growth more efficiently than the monomeric αReps (Fig. 4F,G,J). The microtubule (-) end growth was slowed down already in the presence of only 10 nM $(iiH5)_2$ and completely blocked at 100 nM $(iiH5)_2$. Strikingly, as in the case of the monovalent αReps, the growth of the (+) end remained unaffected up to 1 µM $(iiH5)_2$. At 10 µM $(iiH5)_2$, (+) end growth finally also stopped, i.e. at a concentration about 2 orders of magnitude higher than that needed to block (-) end growth.

From these results, the mechanism of microtubule assembly inhibition by these αReps can be deduced (Fig. 4K). Tubulin–αRep complexes cannot be incorporated at the microtubule (+) end because the longitudinal surface of the α subunit of the incoming tubulin is masked by the αRep. Therefore, at that end, the αReps act as tubulin-sequestering proteins and high αRep concentrations are required to exert an effect. In contrast, αReps may bind at the microtubule (-) end, where α-tubulin subunits are exposed. They may bind on their own but also as a complex with tubulin because the β-tubulin longitudinal surface remains accessible in this complex. In this case, the targeted protofilaments become capped and cannot elongate further. Therefore, as long as an αRep caps the protofilament (-) end, it blocks the association of many incoming tubulins (either in complex with αReps or not). This mechanism explains why the αReps interfere with microtubule growth more drastically at (-) than at (+) ends and interfere selectively with (-) end growth at lower αRep concentrations. This mechanism is reminiscent of that of β-tubulin-targeting DARPins (Pecqueur et al., 2012), but with reverse outcomes at both ends of the microtubule.

The plasticity of α-tubulin.

Although the iE5 and iiH5 αReps share the same mechanism of microtubule inhibition (Fig. 4) and their epitopes on tubulin overlap, the binding modes of the two αReps also clearly differ (Fig. 3F). One consequence was the possibility to engineer $(iiH5)_2$ (Fig. S2) whereas the design of an iE5-based tandem repeat αRep would have been more difficult. The different binding modes also result in an overall surface area buried upon complex formation of about 1650 $Å^2$ in the case of tubulin–iiH5 vs about 2470 $Å^2$ in the case of tubulin–iE5. Interestingly, this larger buried surface does not translate into a higher affinity (Fig. 1D, E). A tubulin conformational change might explain this apparent discrepancy (Kastritis et al., 2011). Indeed, in the complex with iE5, a different conformation of the α-tubulin T7 loop, which interacts with this αRep, is observed. This structural variation propagates to the adjacent H7 and H8 helices (Fig. 5A), while remaining compatible with the binding to tubulin of, e.g., kinesin-1 and colchicine (Fig. S3). The α-tubulin structural change is best pictured by comparing the H7 central helix, which translates when tubulin switches from a straight microtubular conformation to a curved soluble one (Ravelli et al., 2004). After superposition of the secondary structural elements of the N-terminal domain, a translation of about 1 Å is needed to superimpose the α subunit H7 helices of tubulin–iiH5 and tubulin–iE5, which is about half of the translation value when comparing the iiH5 complex and the microtubule (Fig. 5B). This translation is accompanied by changes in the intermediate domain (Fig. 5C). When the comparison is extended to other structures of non-microtubular tubulin, additional positions of the H7 helix that are intermediate between the ones in tubulin–

iiH5 and tubulin–iE5 are found (Fig. 5D). Therefore, the α subunit in tubulin–iE5 is in a conformation that is on the way to the ones observed in the microtubule.

We then questioned whether the structural differences within the α subunit in the complexes with αReps extend to the overall conformation of tubulin. In both complexes, tubulin is in a curved conformation. We calculated angles between the α and β subunits ranging from 10.7° to 12° for the three molecules of the asymmetric unit in the complex with iiH5. In the case of tubulin–iE5, the angle is slightly larger (about 18°), being in the upper range of values found in crystal structures of tubulin (Fig. 5E, Table 3). Therefore, whereas tubulin has a straight conformation in the microtubule core (Nogales et al., 1999; Zhang et al., 2015) and adopts intermediate shapes at microtubule ends (Atherton et al., 2017; Chrétien et al., 1999; Guesdon et al., 2016), the structural results presented here agree with the general view that tubulin is curved when disassembled (Gigant et al., 2000; Melki et al., 1989), with a curvature angle that is at least about 10° (Table 3). Interestingly, although the α subunit in tubulin–iE5 is in a conformation intermediate between that seen in tubulin–iiH5 and the microtubular ones, this complex displays the largest tubulin curvature. This observation suggests that, outside the microtubule context, conformational changes within the subunits are uncorrelated to the variation of the αβ-tubulin curvature.

Conclusion.

In this work, we have selected α-tubulin specific αReps. These binders prevent tubulin self-association by targeting a surface that is involved in longitudinal interactions in tubulin assemblies, with different implications for the two microtubule ends (Fig. 4). Their binding mode is reminiscent of that of the N-terminal β-hairpin of SLDs (Clément et al., 2005; Wang et al., 2012), which also interacts with this tubulin surface (Ravelli et al., 2004). But SLDs stabilize in addition a second tubulin molecule through their C-terminal helix to form a T_2SLD complex (Gigant et al., 2000). Different from this case, the binding site of iE5 and iiH5 αReps is restricted to the α-tubulin longitudinal surface. Therefore, when bound to tubulin, they leave the surface that corresponds to the exterior of the microtubule accessible (Nogales et al., 1999). We anticipate that these α-tubulin-specific αReps will be useful for mechanistic and structural studies of microtubule dynamics and of tubulin:MAPs interactions, and complementary to DARPins that target the β subunit (Pecqueur et al., 2012).

Finally, our results enlighten the plasticity of the tubulin subunits. Interestingly, in microtubules, the α subunit undergoes the most substantial structural variations associated with GTP hydrolysis (Manka and Moores, 2018; Zhang et al., 2015; Zhang et al., 2018). Our data indicate that a conformational change of α-tubulin towards the microtubule structure may be initiated outside the microtubule context. However, the full microtubular conformation has been seen only in microtubules and related assemblies (Löwe et al., 2001; Zhang et al., 2015) and remains to be captured in soluble tubulin complexes.

Acknowledgements

We thank M. Knossow (I2BC, Gif-sur-Yvette) for discussions and critical reading of the manuscript. Diffraction data were collected at the SOLEIL synchrotron (PX1 and PX2 beam lines, Saint-Aubin, France)

and at the European Synchrotron Radiation Facility (ID30 beam line, Grenoble, France). We are most grateful to the machine and beam line groups for making these experiments possible. We thank D. Mauchand (Unité Commune d'Expérimentation Animale, Institut National de la Recherche Agronomique, Jouy en Josas, France) for providing us with the material from which tubulin was purified. This work has benefited from the facilities and expertise of the I2BC crystallization and biophysics platforms. This work has been supported by the Fondation ARC pour la recherche sur le cancer (to B.G.), by CNRS, and by the French Infrastructure for Integrated Structural Biology (FRISBI) ANR-10-INSB-05-01. T.C. and T.S. were supported by the Francis Crick Institute, which receives its core funding from Cancer Research UK (FC001163), the UK Medical Research Council (FC001163), and the Wellcome Trust (FC001163), and by the European Research Council (Advanced Grant, project 323042).

Author contributions

P.M. and B.G. designed research; V.C., A.U., S.C.F. and M.A.N. performed research; V.C., A.U., M.V.L., P.M. and B.G. analyzed data; T.C. and T.S. designed and performed the TIRFM experiments; B.G. wrote the manuscript with input from all authors.

Declaration of Interests

The authors declare no competing interests.

References

Ahmad, S., Pecqueur, L., Dreier, B., Hamdane, D., Aumont-Nicaise, M., Plückthun, A., Knossow, M., and Gigant, B. (2016). Destabilizing an interacting motif strengthens the association of a designed ankyrin repeat protein with tubulin. Sci Rep *6*, 28922.

Atherton, J., Jiang, K., Stangier, M.M., Luo, Y., Hua, S., Houben, K., van Hooff, J.J.E., Joseph, A.P., Scarabelli, G., Grant, B.J., et al. (2017). A structural model for microtubule minus-end recognition and protection by CAMSAP proteins. Nat Struct Mol Biol *24*, 931-943.

Ayaz, P., Munyoki, S., Geyer, E.A., Piedra, F.A., Vu, E.S., Bromberg, R., Otwinowski, Z., Grishin, N.V., Brautigam, C.A., and Rice, L.M. (2014). A tethered delivery mechanism explains the catalytic action of a microtubule polymerase. Elife *3*, e03069.

Ayaz, P., Ye, X., Huddleston, P., Brautigam, C.A., and Rice, L.M. (2012). A TOG:$\alpha\beta$-tubulin complex structure reveals conformation-based mechanisms for a microtubule polymerase. Science *337*, 857-860.

Baker, N.A., Sept, D., Joseph, S., Holst, M.J., and McCammon, J.A. (2001). Electrostatics of nanosystems: application to microtubules and the ribosome. Proc Natl Acad Sci U S A *98*, 10037-10041.

Benoit, M., Asenjo, A.B., and Sosa, H. (2018). Cryo-EM reveals the structural basis of microtubule depolymerization by kinesin-13s. Nat Commun *9*, 1662.

Bieling, P., Telley, I.A., Hentrich, C., Piehler, J., and Surrey, T. (2010). Fluorescence microscopy assays on chemically functionalized surfaces for quantitative imaging of microtubule, motor, and +TIP dynamics. Methods Cell Biol *95*, 555-580.

Bricogne, G., Blanc, E., Brandl, M., Flensburg, C., Keller, P., Paciorek, W., Roversi, P., Sharff, A., Smart, O.S., Vonrhein, C., et al. (2017). BUSTER version 2.10.3 Cambridge, United Kingdom: Global Phasing Ltd.

Cao, L., Wang, W., Jiang, Q., Wang, C., Knossow, M., and Gigant, B. (2014). The structure of apo-kinesin bound to tubulin links the nucleotide cycle to movement. Nat Commun *5*, 5364.

Castoldi, M., and Popov, A.V. (2003). Purification of brain tubulin through two cycles of polymerization-depolymerization in a high-molarity buffer. Protein Expr Purif *32*, 83-88.

Chevrel, A., Mesneau, A., Sanchez, D., Celma, L., Quevillon-Cheruel, S., Cavagnino, A., Nessler, S., Li de la Sierra-Gallay, I., van Tilbeurgh, H., Minard, P., et al. (2018). Alpha repeat proteins (αRep) as expression and crystallization helpers. J Struct Biol *201*, 88-99.

Chrétien, D., Jainosi, I., Taveau, J.C., and Flyvbjerg, H. (1999). Microtubule's conformational cap. Cell Struct Funct *24*, 299-303.

Clément, M.J., Jourdain, I., Lachkar, S., Savarin, P., Gigant, B., Knossow, M., Toma, F., Sobel, A., and Curmi, P.A. (2005). N-terminal stathmin-like peptides bind tubulin and impede microtubule assembly. Biochemistry *44*, 14616-14625.
Desai, A., and Mitchison, T.J. (1997). Microtubule polymerization dynamics. Annu Rev Cell Dev Biol *13*, 83-117.
Dorléans, A., Knossow, M., and Gigant, B. (2007). Studying drug-tubulin interactions by X-ray crystallography. Methods Mol Med *137*, 235-243.
Duellberg, C., Trokter, M., Jha, R., Sen, I., Steinmetz, M.O., and Surrey, T. (2014). Reconstitution of a hierarchical +TIP interaction network controlling microtubule end tracking of dynein. Nat Cell Biol *16*, 804-811.
Emsley, P., Lohkamp, B., Scott, W.G., and Cowtan, K. (2010). Features and development of Coot. Acta Crystallogr D Biol Crystallogr *66*, 486-501.
Gasteiger, E., Hoogland, C., Gattiker, A., Duvaud, S., Wilkins, M.R., Appel, R.D., and Bairoch, A. (2005). Protein identification and analysis tools on the ExPASy server. *In* The Proteomics Protocols Handbook. J.M. Walker, editor. Humana Press. 571-607.
Gigant, B., Curmi, P.A., Martin-Barbey, C., Charbaut, E., Lachkar, S., Lebeau, L., Siavoshian, S., Sobel, A., and Knossow, M. (2000). The 4 Å X-ray structure of a tubulin:stathmin-like domain complex. Cell *102*, 809-816.
Gigant, B., Landrieu, I., Fauquant, C., Barbier, P., Huvent, I., Wieruszeski, J.M., Knossow, M., and Lippens, G. (2014). Mechanism of Tau-promoted microtubule assembly as probed by NMR spectroscopy. J Am Chem Soc *136*, 12615-12623.
Gigant, B., Wang, W., Dreier, B., Jiang, Q., Pecqueur, L., Pluckthun, A., Wang, C., and Knossow, M. (2013). Structure of a kinesin-tubulin complex and implications for kinesin motility. Nat Struct Mol Biol *20*, 1001-1007.
Guellouz, A., Valerio-Lepiniec, M., Urvoas, A., Chevrel, A., Graille, M., Fourati-Kammoun, Z., Desmadril, M., van Tilbeurgh, H., and Minard, P. (2013). Selection of specific protein binders for pre-defined targets from an optimized library of artificial helicoidal repeat proteins (alphaRep). PLoS One *8*, e71512.
Guesdon, A., Bazile, F., Buey, R.M., Mohan, R., Monier, S., Garcia, R.R., Angevin, M., Heichette, C., Wieneke, R., Tampe, R., et al. (2016). EB1 interacts with outwardly curved and straight regions of the microtubule lattice. Nat Cell Biol *18*, 1102-1108.
Howes, S.C., Geyer, E.A., LaFrance, B., Zhang, R., Kellogg, E.H., Westermann, S., Rice, L.M., and Nogales, E. (2017). Structural differences between yeast and mammalian microtubules revealed by cryo-EM. J Cell Biol *216*, 2669-2677.
Hyman, A., Drechsel, D., Kellogg, D., Salser, S., Sawin, K., Steffen, P., Wordeman, L., and Mitchison, T. (1991). Preparation of modified tubulins. Methods Enzymol *196*, 478-485.
Johnson, V., Ayaz, P., Huddleston, P., and Rice, L.M. (2011). Design, overexpression, and purification of polymerization-blocked yeast $\alpha\beta$-tubulin mutants. Biochemistry *50*, 8636-8644.
Jourdain, L., Curmi, P., Sobel, A., Pantaloni, D., and Carlier, M.F. (1997). Stathmin: a tubulin-sequestering protein which forms a ternary T2S complex with two tubulin molecules. Biochemistry *36*, 10817-10821.
Kabsch, W. (2010). XDS. Acta Crystallogr D Biol Crystallogr *66*, 125-132.
Kastritis, P.L., Moal, I.H., Hwang, H., Weng, Z., Bates, P.A., Bonvin, A.M., and Janin, J. (2011). A structure-based benchmark for protein-protein binding affinity. Protein Sci *20*, 482-491.
Legrand, P. (2017). XDSME: XDS Made Easier. GitHub repository, DOI 10.5281/zenodo.837885.
Li, X.H., Culver, J.A., and Rhoades, E. (2015). Tau binds to multiple tubulin dimers with helical structure. J Am Chem Soc *137*, 9218-9221.
Löwe, J., Li, H., Downing, K.H., and Nogales, E. (2001). Refined structure of $\alpha\beta$-tubulin at 3.5 Å resolution. J Mol Biol *313*, 1045-1057.
Manka, S.W., and Moores, C.A. (2018). The role of tubulin-tubulin lattice contacts in the mechanism of microtubule dynamic instability. Nat Struct Mol Biol *25*, 607-615.
Maurer, S.P., Cade, N.I., Bohner, G., Gustafsson, N., Boutant, E., and Surrey, T. (2014). EB1 accelerates two conformational transitions important for microtubule maturation and dynamics. Curr Biol *24*, 372-384.
McCoy, A.J., Grosse-Kunstleve, R.W., Adams, P.D., Winn, M.D., Storoni, L.C., and Read, R.J. (2007). Phaser crystallographic software. J Appl Crystallogr *40*, 658-674.
Melki, R., Carlier, M.F., Pantaloni, D., and Timasheff, S.N. (1989). Cold depolymerization of microtubules to double rings: geometric stabilization of assemblies. Biochemistry *28*, 9143-9152.

Mignot, I., Pecqueur, L., Dorleans, A., Karuppasamy, M., Ravelli, R.B., Dreier, B., Pluckthun, A., Knossow, M., and Gigant, B. (2012). Design and characterization of modular scaffolds for tubulin assembly. J Biol Chem *287*, 31085-31094.
Minoura, I., Hachikubo, Y., Yamakita, Y., Takazaki, H., Ayukawa, R., Uchimura, S., and Muto, E. (2013). Overexpression, purification, and functional analysis of recombinant human tubulin dimer. FEBS Lett *587*, 3450-3455.
Nawrotek, A., Guimarães, B.G., Velours, C., Subtil, A., Knossow, M., and Gigant, B. (2014). Biochemical and structural insights into microtubule perturbation by CopN from *Chlamydia pneumoniae*. J Biol Chem *289*, 25199-25210.
Nawrotek, A., Knossow, M., and Gigant, B. (2011). The determinants that govern microtubule assembly from the atomic structure of GTP-tubulin. J Mol Biol *412*, 35-42.
Nogales, E., and Kellogg, E.H. (2017). Challenges and opportunities in the high-resolution cryo-EM visualization of microtubules and their binding partners. Curr Opin Struct Biol *46*, 65-70.
Nogales, E., Whittaker, M., Milligan, R.A., and Downing, K.H. (1999). High-resolution model of the microtubule. Cell *96*, 79-88.
Pecqueur, L., Duellberg, C., Dreier, B., Jiang, Q., Wang, C., Plückthun, A., Surrey, T., Gigant, B., and Knossow, M. (2012). A designed ankyrin repeat protein selected to bind to tubulin caps the microtubule plus end. Proc Natl Acad Sci U S A *109*, 12011-12016.
Plückthun, A. (2015). Designed ankyrin repeat proteins (DARPins): binding proteins for research, diagnostics, and therapy. Annu Rev Pharmacol Toxicol *55*, 489-511.
Prota, A.E., Bargsten, K., Zurwerra, D., Field, J.J., Diaz, J.F., Altmann, K.H., and Steinmetz, M.O. (2013a). Molecular mechanism of action of microtubule-stabilizing anticancer agents. Science *339*, 587-590.
Prota, A.E., Magiera, M.M., Kuijpers, M., Bargsten, K., Frey, D., Wieser, M., Jaussi, R., Hoogenraad, C.C., Kammerer, R.A., Janke, C., et al. (2013b). Structural basis of tubulin tyrosination by tubulin tyrosine ligase. J Cell Biol *200*, 259-270.
Ravelli, R.B., Gigant, B., Curmi, P.A., Jourdain, I., Lachkar, S., Sobel, A., and Knossow, M. (2004). Insight into tubulin regulation from a complex with colchicine and a stathmin-like domain. Nature *428*, 198-202.
Roostalu, J., Cade, N.I., and Surrey, T. (2015). Complementary activities of TPX2 and chTOG constitute an efficient importin-regulated microtubule nucleation module. Nat Cell Biol *17*, 1422-1434.
Sharma, A., Aher, A., Dynes, N.J., Frey, D., Katrukha, E.A., Jaussi, R., Grigoriev, I., Croisier, M., Kammerer, R.A., Akhmanova, A., et al. (2016). Centriolar CPAP/SAS-4 imparts slow processive microtubule growth. Dev Cell *37*, 362-376.
Ti, S.C., Pamula, M.C., Howes, S.C., Duellberg, C., Cade, N.I., Kleiner, R.E., Forth, S., Surrey, T., Nogales, E., and Kapoor, T.M. (2016). Mutations in human tubulin proximal to the kinesin-binding site alter dynamic instability at microtubule plus- and minus-ends. Dev Cell *37*, 72-84.
Urvoas, A., Guellouz, A., Valerio-Lepiniec, M., Graille, M., Durand, D., Desravines, D.C., van Tilbeurgh, H., Desmadril, M., and Minard, P. (2010). Design, production and molecular structure of a new family of artificial alpha-helicoidal repeat proteins (αRep) based on thermostable HEAT-like repeats. J Mol Biol *404*, 307-327.
Vemu, A., Atherton, J., Spector, J.O., Szyk, A., Moores, C.A., and Roll-Mecak, A. (2016). Structure and dynamics of single-isoform recombinant neuronal human tubulin. J Biol Chem *291*, 12907-12915.
Wang, W., Cantos-Fernandes, S., Lv, Y., Kuerban, H., Ahmad, S., Wang, C., and Gigant, B. (2017). Insight into microtubule disassembly by kinesin-13s from the structure of Kif2C bound to tubulin. Nat Commun *8*, 70.
Wang, W., Jiang, Q., Argentini, M., Cornu, D., Gigant, B., Knossow, M., and Wang, C. (2012). Kif2C minimal functional domain has unusual nucleotide binding properties that are adapted to microtubule depolymerization. J Biol Chem *287*, 15143-15153.
Zhang, R., Alushin, G.M., Brown, A., and Nogales, E. (2015). Mechanistic origin of microtubule dynamic instability and its modulation by EB proteins. Cell *162*, 849-859.
Zhang, R., LaFrance, B., and Nogales, E. (2018). Separating the effects of nucleotide and EB binding on microtubule structure. Proc Natl Acad Sci U S A *115*, E6191-E6200.

Figure legends

Figure 1. The iE5 and iiH5 αReps bind tubulin and inhibit microtubule assembly. (A) Strategy for the selection of α-tubulin-specific αReps. A biotinylated version of the β-tubulin-specific DARPin A-C2 (Ahmad et al., 2016) was trapped on a streptavidin-coated plate, making the α subunit of bound tubulin most exposed. (B) Gel filtration profile of 20 µM tubulin alone or in presence of 40 µM of either iE5 or iiH5. See also Fig. S3A. (C) Fractions defined at the top of panel B were submitted to SDS-PAGE, which confirms the formation of tubulin–αRep complexes. Irrelevant lanes have been removed from the upper gel. T, tubulin. (D,E) ITC analysis of the interaction between tubulin and iE5 (D) or iiH5 (E). Experiments were performed by stepwise titration of the αRep (160 µM concentration) into 15 µM tubulin. Upper panels display raw data; lower panels show the integrated heat changes and associated curve fits, from which the indicated K_D values were extracted. (F,G) iE5 and iiH5 inhibit microtubule assembly in a dose-dependent manner. The assembly of 20 µM tubulin in presence of increasing concentrations of iE5 (F) or iiH5 (G), as indicated, is compared with the assembly of 10, 15 and 20 µM tubulin alone. Microtubule assembly was monitored by turbidity. The temperature was switched from 5 to 37 °C after 1 min of recording time in each case and the arrowhead indicates the reverse temperature switch. In the case of iiH5, the assembly buffer was supplemented with 75 mM KCl to avoid aggregation. (H) The $(iiH5)_2$ tandem repeat αRep (see Fig. S2) inhibits microtubule assembly. The assembly of tubulin (20 or 30 µM) in presence of $(iiH5)_2$ at the indicated concentrations was monitored by turbidity in the conditions used in panel G, from which the tubulin control curves are taken.

Figure 2. The tubulin–iE5 structure. (A) Overview of the complex crystallized. The iE5 internal repeats are in orange, and the N-cap and C-cap are in yellow. The α-tubulin secondary structural elements (defined in Fig. S1) that interact with iE5 are in magenta. (B) Electrostatic potential surface of tubulin, with bound iE5 shown as a cartoon model. (C) iE5 prevents inter-tubulin longitudinal interactions. iE5 (surface representation) has been modeled on a microtubule α subunit (magenta) after superposition of α-tubulin from tubulin–iE5. iE5 would clash with the β subunit (bright green) of a neighboring tubulin along a protofilament. View from the outside of the microtubule (pdb id 3JAK (Zhang et al., 2015); 2 tubulin segments of 3 protofilaments are traced). (D) Electrostatic potential surface of iE5, with the interacting α-tubulin elements shown in magenta. (E) Sequence of iE5. The residues at randomized positions are in red. The residues that are less than 5 Å distant from tubulin residues in the complex are highlighted in cyan (invariant residues) or in green (randomized positions).

Figure 3. The tubulin–iiH5 structure. (A) Overview of the complex crystallized. (B) Tubulin–iiH5 forms a helical assembly of 6 complexes per turn in the crystal. (C) Electrostatic potential surface of tubulin, with bound iiH5 shown as a cartoon model. (D) Electrostatic potential surface of iiH5, with the α-tubulin elements that interact with iiH5 shown in magenta. (E) Sequence of iiH5. See Fig. 2E for color code explanations. (F) Comparison of the tubulin binding modes of iE5 and iiH5 αReps. The α subunit from tubulin–iiH5 has been superimposed to that from tubulin–iE5; only the latter is shown.

Figure 4. The αReps selectively inhibit microtubule (-) end growth. (A-G) Representative TIRFM kymographs showing individual microtubules growing from surface-immobilized GMPCPP 'seeds' in the absence (A) or presence of iE5 (B,C), iiH5 (D,E) and $(iiH5)_2$ (F,G) αReps at the indicated concentrations.

Experiments were performed at 30 °C in presence of 15 µM CF640R-labeled tubulin. Scale bars, 6 µm (horizontal), 2 min (vertical). (H-J) Mean growth velocities of microtubule (+) and (-) ends (black and magenta symbols, respectively) as a function of iE5 (H), iiH5 (I) and $(iiH5)_2$ (J) αRep concentration. At least 20 microtubules per condition were used for growth speed measurements. Error bars are SD. (K) Model of microtubule assembly inhibition by the $(iiH5)_2$ tandem repeat αRep. The tubulin–$(iiH5)_2$ complex is not incorporated at the (+) end, which continues growing as long as enough free tubulin is available. By contrast, $(iiH5)_2$ or the complex it forms with tubulin associates at the (-) end but then blocks addition of tubulin heterodimers to capped protofilaments.

Figure 5. The α-tubulin plasticity. (A) α-tubulin differences in the iE5 and iiH5 complexes. The α subunit of tubulin–iE5 has been superimposed to that of tubulin–iiH5, taking the secondary structural elements of the N-terminal domain as a reference (see Fig. S1). α-tubulin bound to iE5 is in pink, with the regions that interact with the αRep in magenta; iE5 is in orange. α-tubulin from tubulin–iiH5 is in cyan, with the H7-T7-H8 region in brighter color and intermediate domain structural elements in blue; iiH5 is not shown. For clarity, the α-tubulin N-terminal H1-S2 loop is not traced. (B) Comparison of α-tubulin in the iiH5 complex (cyan and blue), in tubulin–iE5 (pink and magenta) and in the microtubule (grey; pdb id 3JAK), centered on the H7 helix. The α subunits have been aligned as in panel A. (C) Same as in panel B, but only the α-tubulin intermediate domain β sheet is depicted. (D) Comparison of α-tubulin H7 position in different structures after superposition as in panel A, taking tubulin–iiH5 as a reference. The comparison is with microtubular tubulin (pdb id 3JAK) and with T_2SLD (pdb id 3RYC; (Nawrotek et al., 2011)). (E) Comparison of the overall conformation of αβ-tubulin bound to iiH5 (grey) and to iE5 (pink and green). After superposing the α subunits, the β subunits are misaligned by about 7°. As the tubulin β subunit is the part of this protein that is most distant from the αRep in the complexes described here, this misalignment is most likely solely due to the crystal packing.

Table 1. Thermodynamic binding parameters determined by ITC

αReps	n	K_D (nM)	ΔH (kcal mol^{-1})	TΔS (kcal mol^{-1})	ΔG (kcal mol^{-1})
iE5	0.8	270 ± 75	-8	-0.4	-8.4
iiH5	1	95 ± 15	-16	7	-9

Table 2. Data collection and refinement statistics.

	Tubulin–iE5	Tubulin–iiH5
Data collection[(a)]		
Space group	$P3_221$	C2
Cell dimensions		
a, b, c (Å)	102.3, 102.3, 216.2	450.8, 53.8, 229.6
α, β, γ(°)	90.0, 90.0, 120.0	90.0, 118.8, 90.0
Resolution (Å)	46.2-2.60 (2.69-2.60)	36.8-3.20 (3.31-3.20)
R_{meas}	0.169 (1.95)	0.321 (1.05)
I / σI	14.6 (1.2)	4.17 (1.02)
$CC_{1/2}$	0.999 (0.446)	0.954 (0.569)
Completeness	99.9 (100)	98.9 (98.2)
Multiplicity	13.2 (12.5)	3.2 (3.3)
Refinement		
Resolution (Å)	46.2-2.60	36.85-3.20
No. reflections	41238	80684
Rwork / Rfree	0.173 / 0.223	0.230 (0.270)
Number of non-hydrogen atoms		
Protein	8202	23796
Ligands	100	183
Solvent	176	0
B factors		
Protein	70.6	90.6
Ligands	75.3	89.4
Solvent	60.2	
Coordinate error (Å)	0.31	0.61
R.m.s.d.		
Bond lengths (Å)	0.010	0.010
Bond angles (°)	1.16	1.20
Ramachandran (%)		
Favored region	97.15	94.03
Allowed region	2.66	4.98
Outliers	0.19	0.99

[(a)] Data were collected on a single crystal. Values in parentheses are for the highest-resolution shell.

Table 3. Angle between the α and β subunits in a subset of tubulin structures[a].

	Angle value	pdb id
Microtubule	1.1°	3JAK
Tubulin–kinesin–DARPin	9.2°	4HNA
Tubulin–SLD–TTL	10.5°	4I4T
Tubulin–SLD	10.6°	3RYC
Tubulin–SLD–DARPin	10.6°	4F6R
Tubulin–iiH5[b]	11.2°	6GWD[c]
Tubulin–kinesin–DARPin	11.6°	4LNU
Tubulin–DARPin	11.9°	4DRX
Tubulin–TOG	12.2°	4U3J
Tubulin–TOG	13.5°	4FFB
Tubulin–DARPin	13.5°	5EYP
Tubulin–CPAP–DARPin	14.4°	5ITZ
Tubulin–kinesin–DARPin	14.7°	5MIO
Tubulin–iE5	18.2°	6GWC[c]

[a] Obtained by superposing the secondary structural elements of the N-terminal domain of α-tubulin to those of β-tubulin, as defined in Fig. S1.
[b] Average value for the 3 molecules of the asymmetric unit.
[c] This work.

STAR METHODS.

CONTACT FOR REAGENT AND RESOURCE SHARING

Further information and requests for resources and reagents should be directed to and will be fulfilled by the Lead Contact, Benoît Gigant (benoit.gigant@i2bc.paris-saclay.fr)

EXPERIMENTAL MODEL AND SUBJECT DETAILS

αRep library. Anti-tubulin αReps were selected from the 2.1 optimized αRep library (Guellouz et al., 2013).

Bacteria strains. XL1-Blue, Bl21(DE3) and Bl21(DE3)STAR cells were cultured in 2YT medium in the presence of appropriate antibiotics.

METHOD DETAILS

αRep selection. αRep selection was performed by phage display essentially following published procedures (Guellouz et al., 2013). To immobilize tubulin, the gene coding for the high-affinity tubulin-binding DARPin A-C2 (Ahmad et al., 2016) was modified to introduce an AviTag biotinylation coding sequence at the C-terminal end of the protein. Modified A-C2 was expressed in *E. coli* Bl21(DE3)STAR co-transformed with the pBirAcm plasmid (Avidity, LLC, USA) for in vivo biotinylation and purified as described for non-biotinylated A-C2 (Ahmad et al., 2016). Tubulin was trapped through its interaction with biotinylated A-C2 that was immobilized on a streptavidin-coated plate (Fig. 1A). After each round of selection, bound phages eluted either in acidic conditions or more specifically by adding DARPin or tubulin were amplified in XL1-Blue cells and used for the following selection round. After 3 rounds, individual clones were screened for tubulin binding by phage-ELISA (Guellouz et al., 2013).

Protein purification. αRep genes were subcloned in pQE-81L plasmid (Qiagen) for expression in *E. coli* Bl21(DE3) in 2YT medium at 37 °C. After sonication of the bacteria suspension, αReps were purified from the soluble fraction by Ni^{2+}-affinity chromatography (Histrap HP, GE Healthcare) followed by gel filtration (Superdex 75 16/60 HL, GE Healthcare) in 20 mM Pipes-K, pH 6.8, 1 mM $MgCl_2$, 0.5 mM EGTA and 150 mM KCl. In the case of iiH5, the storage buffer contained 500 mM KCl. The $(iiH5)_2$ tandem repeat αRep (Fig. S2; Campanacci et al, submitted) was produced and purified as iiH5. The concentration of αReps was estimated by UV spectrophotometry using theoretical extinction coefficients at 280 nm (Gasteiger et al., 2005). Tubulin was purified by two cycles of assembly in a high-molarity buffer followed by disassembly (Castoldi and Popov, 2003). Sheep brain tubulin was used throughout, except for the TIRFM experiments which were performed with porcine brain tubulin. Before use, an additional cycle of assembly and disassembly was performed to remove inactive protein. To prepare the tubulin–colchicine complex used in Fig. S3, colchicine was included in the disassembly buffer (Dorléans et al., 2007). The motor domain of the human kinesin-1 Kif5B (cys-light construct, comprising residues 1 to 349) was produced and purified as described (Cao et al., 2014).

Size exclusion chromatography. Samples were analyzed on a Superdex 200 10/300 GL column (GE Healthcare) equilibrated with 20 mM Pipes-K, pH 6.8, 1 mM $MgCl_2$, 0.5 mM EGTA and 150 mM KCl, unless otherwise mentioned. The content of the chromatographic peaks was analyzed by SDS-PAGE with Coomassie Blue staining.

Isothermal titration calorimetry. Calorimetric experiments were conducted at 20 °C with a MicroCal ITC200 instrument (Malvern). All proteins were buffer-exchanged to 20 mM Pipes-K pH 6.8, 1 mM $MgCl_2$, 0.01 mM EGTA, 0.01 mM GDP and 75 mM KCl. Aliquots (2 µL) of iE5 or iiH5 at 160 µM were injected into a 15 µM tubulin solution (cell volume, 0.24 mL). Analysis of the data was performed using the MicroCal Origin software provided by the manufacturer according to the one-binding-site model.

Microtubule assembly inhibition. Microtubule assembly was performed in a buffer consisting of 50 mM Mes-K, pH 6.8, 6 mM $MgCl_2$, 1 mM EGTA, 30% (v/v) glycerol, and 0.5 mM GTP. It was initiated by raising the temperature from 5 °C to 37 °C and monitored at 350 nm with a Cary 50 spectrophotometer (Agilent Technologies), using a 0.7-cm path length cuvette. In presence of iiH5 and of $(iiH5)_2$, to avoid aggregation, the assembly buffer was supplemented with 75 mM KCl.

Total internal reflection fluorescence microscopy.

Tubulin was labeled with CF640R-N-hydroxysuccinimide ester (NHS, Sigma-Aldrich) or biotin-NHS ester (Thermo scientific) (Hyman et al., 1991). Flow chambers for TIRF experiments were assembled from polyethylene glycol (PEG)-passivated functionalized glass and poly(L-lysine)-PEG (SuSoS)-passivated counter glass (Bieling et al., 2010). Biotin-PEG-coated glass was prepared by mixing 91% hydroxyl-PEG-3000-amine and 9% biotin-PEG-3000-amine (both from RAPP Polymere) and coupling this mixture to glass. Fluorescently-labeled biotinylated GMPCPP-stabilized microtubule 'seeds' (containing 20% CF640R-labeled tubulin) for assays with dynamic microtubules were prepared as described (Bieling et al., 2010; Roostalu et al., 2015).

The assay was performed essentially as described earlier (Roostalu et al., 2015). In brief, flow chambers were incubated with 5% Pluronic F-127 in MQ water (Sigma-Aldrich) for 10 min at room temperature, washed with assay buffer (AB: 80 mM Pipes, 75 mM KCl, 1 mM EGTA, 1 mM $MgCl_2$, 1 mM GTP, 5 mM 2-mercaptoethanol, 0.15% (w/v) methylcellulose (4,000 cP; Sigma-Aldrich), 1% (w/v) glucose, 0.02% (v/v) Brij-35) supplemented with 50 µg mL^{-1} κ-casein (Sigma-Aldrich). Chambers were subsequently incubated with the same buffer additionally containing 50 µg mL^{-1} NeutrAvidin (Life Technologies) for 3 min on a metal block on ice, washed with AB and then incubated with AB containing an appropriate dilution of fluorescently-labeled GMPCPP-microtubule 'seeds' for 3 min at room temperature. Unbound 'seeds' were removed by additional washes with AB followed by the final assay mixture: 50% (v/v) 2x AB, 48.18% BRB80 (80 mM Pipes, 1 mM EGTA, 1 mM $MgCl_2$) supplemented with oxygen scavengers (682 µg/mL^{-1} glucose oxidase (Serva), 164 µg/mL^{-1} catalase (Sigma-Aldrich)) and 15 µM CF640R-labeled tubulin (labeling ratio: 6.5%), and 1.8% of varying concentrations of □-Reps diluted in their storage buffers. Flow chambers were sealed with vacuum grease (Beckman) and imaging was started 90 s after placing the chamber on the microscope. Experiments were performed at 30 °C ± 1 °C on a TIRF microscope (iMIC, FEI Munich) described in detail previously (Duellberg et al., 2014; Maurer et al., 2014). Image acquisition was carried out as described before (Duellberg et al., 2014; Maurer et al., 2014). All time-lapse movies were recorded at 1 frame per 5 s with a 200-ms exposure time. CF640R-labeled microtubules were excited at 640 nm keeping the laser power constant for all experiments. Mean microtubule growth speeds were calculated from kymographs generated using ImageJ.

Crystallization and structure determination.

Tubulin–iE5 was crystallized at 293 K by vapor diffusion in a crystallization buffer consisting of 13% (v/v) PEG 400, 0.1 M Mes-K pH 6.8. Crystals were harvested in a mother liquor containing 20% PEG 400 and flash-cooled in liquid nitrogen. Tubulin–iiH5 crystals were obtained at 277 K in 0.2 M Na tartrate, 12% (w/v) PEG 3350 and cryoprotected in mother liquor supplemented with 20% glycerol. Datasets were collected at 100 K at the Proxima-1 beamline (SOLEIL Synchrotron, Saint-Aubin, France). Data were processed with XDS (Kabsch, 2010) using the XDSME package (Legrand, 2017). Structures were solved by molecular replacement with Phaser (McCoy et al., 2007) using tubulin (pdb id 4DRX) and Rep-n4-a (pdb id 3LTJ) as search models, and refined with BUSTER (Bricogne et al., 2017) with iterative model building in Coot (Emsley et al., 2010). Data collection and refinement statistics are reported in Table 2. Figures of structural models were generated with PyMOL (www.pymol.org). The electrostatic potential surface was calculated using APBS (Baker et al., 2001) and rendered in PyMOL.

QUANTIFICATION AND STATISTICAL ANALYSIS

Table 2 contains quantitative parameters related to data and refinement statistics. The uncertainty on the K_D determined by ITC (Table 1) was estimated by the Origin software using the Levenberg-Marquardt algorithm. Error bars in the TIRFM experiments (Fig. 4 H-J) are SD from measurements of at least 20 microtubules.

DATA AND SOFTWARE AVAILABILITY

Coordinates and structure factors have been deposited in the Protein Data Bank under accession codes 6GWC (tubulin–iE5) and 6GWD (tubulin–iiH5).

Supplemental Legend

Figure S1. Sequences of α- and β-tubulin, secondary structure assignments and domain definition, Related to Figures 2, 3 and 5. (Top) The sequences of the *Bos taurus* α1B and β2B tubulin isotypes have been aligned as in (Löwe et al., 2001). These sequences were used to refine the tubulin–iE5 and tubulin–iiH5 structures because, to the best of our knowledge, those of *Ovis aries* tubulin are not known. The secondary structure nomenclature is as in (Löwe et al., 2001) and the boundaries of the helices (highlighted in cyan) and strands (yellow) were determined with Pymol from the following structures: pdb id 6GWC (this work), 5EYP (Ahmad et al., 2016), and 4I4T (Prota et al., 2013a), which comprises a helical motif in the M loop as shown here. (Bottom) Tubulin domains. The α subunit (pdb id 5EYP) is shown. The secondary structure elements of its N-terminal domain are in green, with the strands in brighter color; those of the intermediate domain are in pink; and the helices of the C-terminal domain are in cyan. The H7 helix is in yellow and the M loop in magenta.

Figure S2. Design of the $(iiH5)_2$ tandem repeat αRep, Related to Figures 1H, 3 and 4. (A,B) Model of iiH5 bound at the (-) end of a microtubule. This model was obtained by superposing α-tubulin in tubulin–iiH5 to α-tubulin in the microtubule structure (pdb id 3JAK). Four protofilaments are drawn, two of them being decorated by a iiH5 molecule. Views from the inside of the microtubule (A) and along the microtubule axis (B). Color code as in Fig. 3A except that the C-cap of iiH5 is in lighter cyan. (C) Same orientation as in

panel B, but only the two iiH5 molecules are shown. (D) Design of $(iiH5)_2$. To build the tandem repeat αRep, the C-cap of one αRep was removed and the C-terminal end of its last internal HEAT repeat was linked to the N-terminal end of the N-cap of the second one using a $(GGGGS)_3$-GGS motif (dashed line).

Figure S3. iE5 interacts with tubulin bound to colchicine or to kinesin-1, Related to Figures 1B and 5. (A) iE5 and iiH5 interact with the tubulin–colchicine complex. Gel filtration profile in 20 mM Pipes-K, pH 6.8, 1 mM $MgCl_2$, and 0.5 mM EGTA, of 20 µM tubulin–colchicine alone (black lines) or with 80 µM iE5 (blue) or iiH5 (magenta). The absorbance signal of colchicine at 351 nm is also shown (dashed lines). (B,C) iE5 makes a ternary complex with tubulin and kinesin-1. (B) Gel filtration profile in the buffer used in panel A of tubulin (20 µM), of kinesin-1 motor domain (30 µM), or of different mixtures of tubulin, kinesin, and iE5 (80 µM), as indicated. The main chromatographic peak of the tubulin:iE5:kinesin sample is shifted compared to those of tubulin:kinesin and tubulin:iE5, indicating the formation of the ternary complex. (C) Fractions defined at the top of panel B were submitted to SDS-PAGE in the case of tubulin:kinesin (Left) and tubulin:iE5:kinesin (Right), confirming the formation of a ternary complex in this last case.

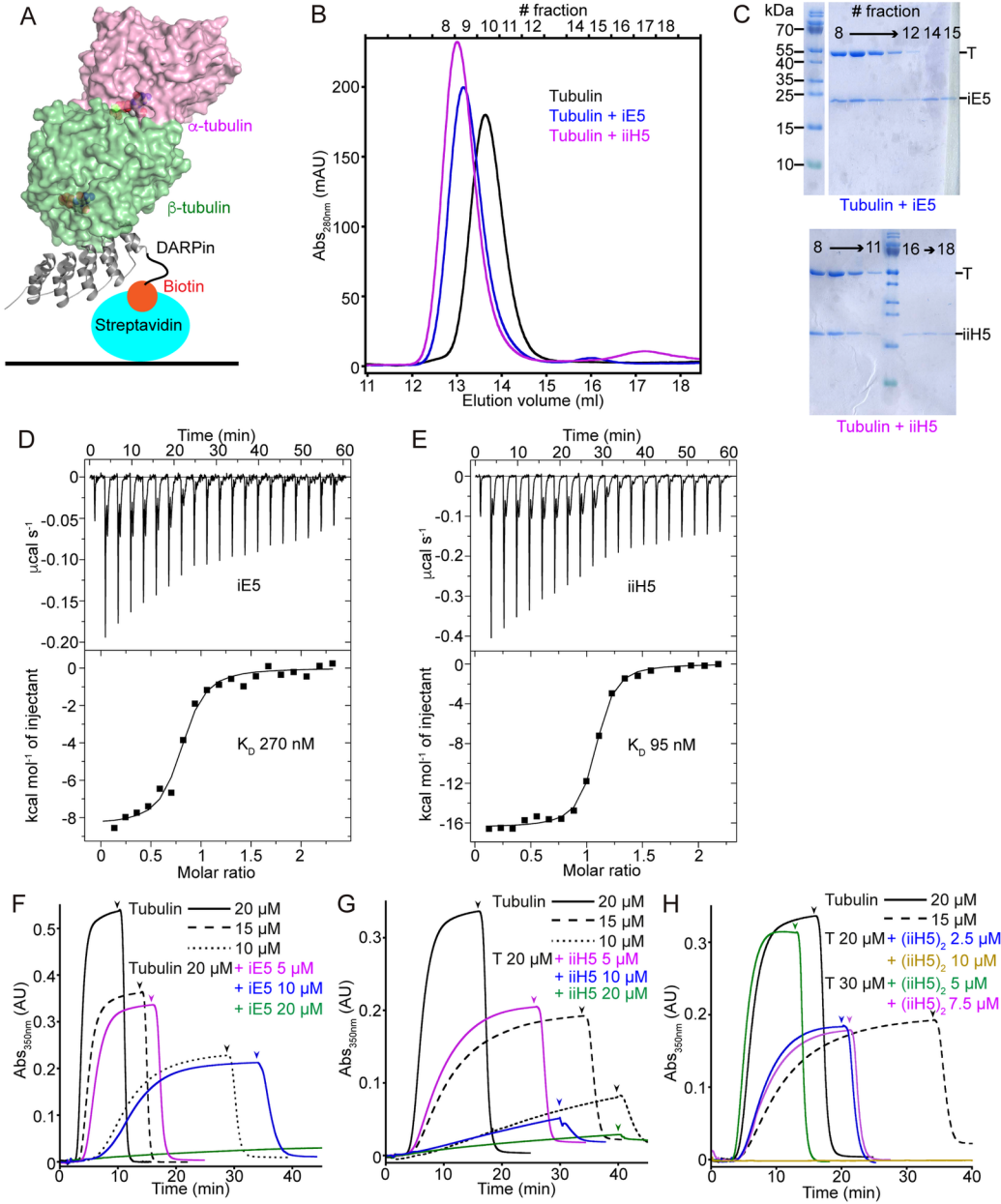
A
α-tubulin
β-tubulin
DARPin
Biotin
Streptavidin
B
fraction
8 9 10 11 12 14 15 16 17 18
Tubulin
Tubulin + iE5
Tubulin + iiH5
Abs280nm (mAU)
Elution volume (ml)
C
kDa
fraction
8 → 12 14 15
T
iE5
Tubulin + iE5
8 → 11 16 → 18
T
iiH5
Tubulin + iiH5
D
Time (min)
µcal s-1
iE5
kcal mol-1 of injectant
KD 270 nM
Molar ratio
E
Time (min)
µcal s-1
iiH5
kcal mol-1 of injectant
KD 95 nM
Molar ratio
F
Tubulin 20 µM
15 µM
10 µM
Tubulin 20 µM + iE5 5 µM
+ iE5 10 µM
+ iE5 20 µM
Abs350nm (AU)
Time (min)
G
Tubulin 20 µM
15 µM
10 µM
T 20 µM + iiH5 5 µM
+ iiH5 10 µM
+ iiH5 20 µM
Abs350nm (AU)
Time (min)
H
Tubulin 20 µM
15 µM
T 20 µM + (iiH5)2 2.5 µM
+ (iiH5)2 10 µM
T 30 µM + (iiH5)2 5 µM
+ (iiH5)2 7.5 µM
Abs350nm (AU)
Time (min)

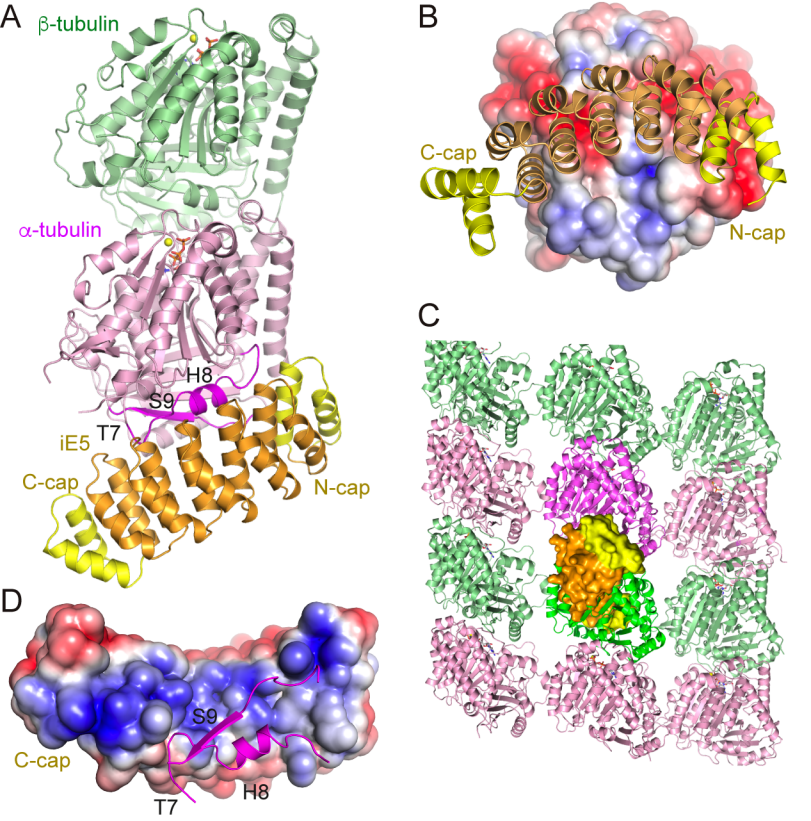

E

1	MRGSHHHHHHTDP.....	Expression tag
14	EKVEMYIKNLQDDSTLVRSIAAAALGKI	N-cap
42	GDERAVEPLIKALKDEDSRVRAQAAGALGQI	Internal Repeats
73	GDERAVEPLIKALKDEDPSVRYRAAEALGKI	
104	GDERAVEPLIKALKDEDTTVRRIAATALGKI	
135	GDERAVEPLIKALKDEDAAVRLTAARALGEI	
166	GDERAVEPLIKALKDEDAYVRRAAAQALGKI	
197	GGERVRAAMEKLAETGTGFARKVAVNYLETHKSLIS..C-cap	

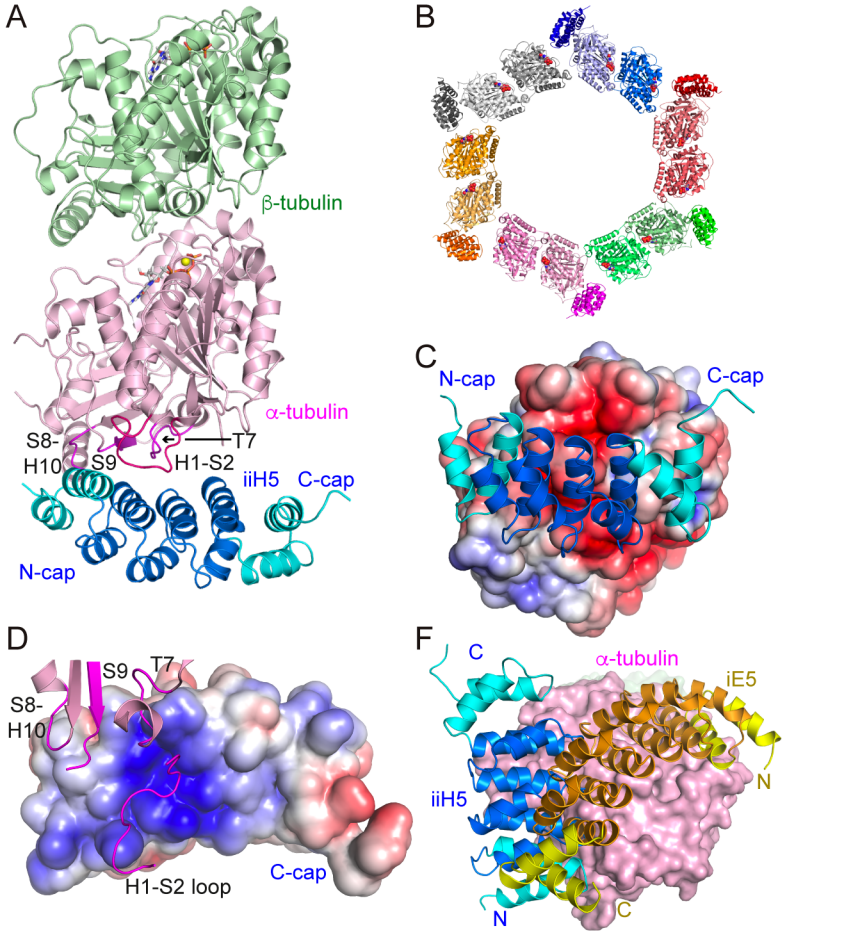

E

```
1     MRGSHHHHHHTDP.........................Expression tag
14    EKVEMYIKNLQDDSPPVRFNAAVALGKI .........N-cap
42    GDERAVEPLIKALKDEDWQVRKTAALALGKI       |  Internal
73    GDERAVEPLIKALKDEDRYVRSRAALALGKI       |  Repeats
104   GDERAVEPLIKALKDEDEYVRLSAASALGKI       |
135   GGERVRAAMEKLAETGTGFARKVAVNYLETHKSLIS..C-cap
```

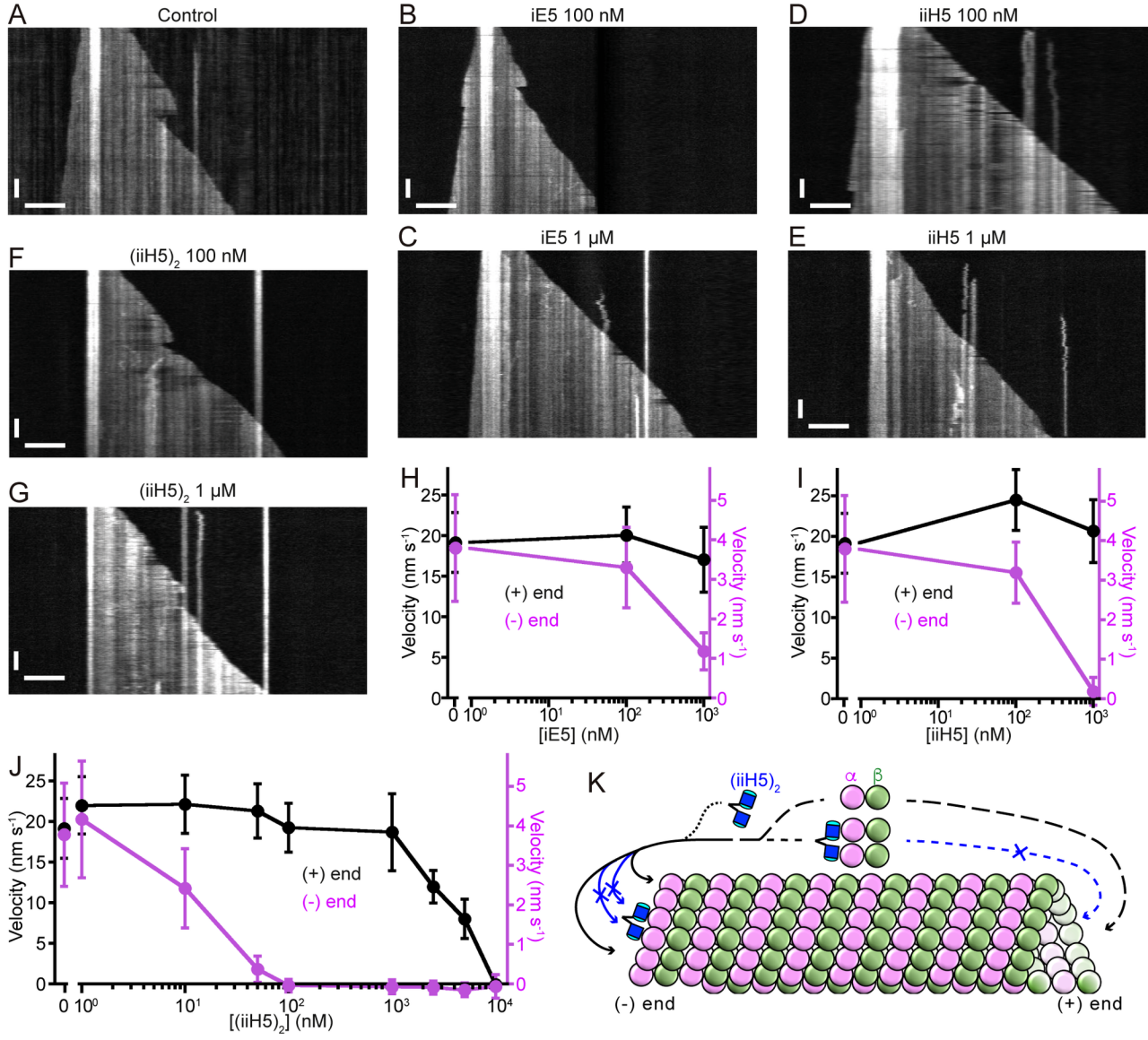
A
Control
B
iE5 100 nM
D
iiH5 100 nM
F
(iiH5)2 100 nM
C
iE5 1 µM
E
iiH5 1 µM
G
(iiH5)2 1 µM
H
Velocity (nm s-1)
Velocity (nm s-1)
(+) end
(-) end
[iE5] (nM)
I
Velocity (nm s-1)
Velocity (nm s-1)
(+) end
(-) end
[iiH5] (nM)
J
Velocity (nm s-1)
Velocity (nm s-1)
(+) end
(-) end
[(iiH5)2] (nM)
K
(iiH5)2
α
β
(-) end
(+) end

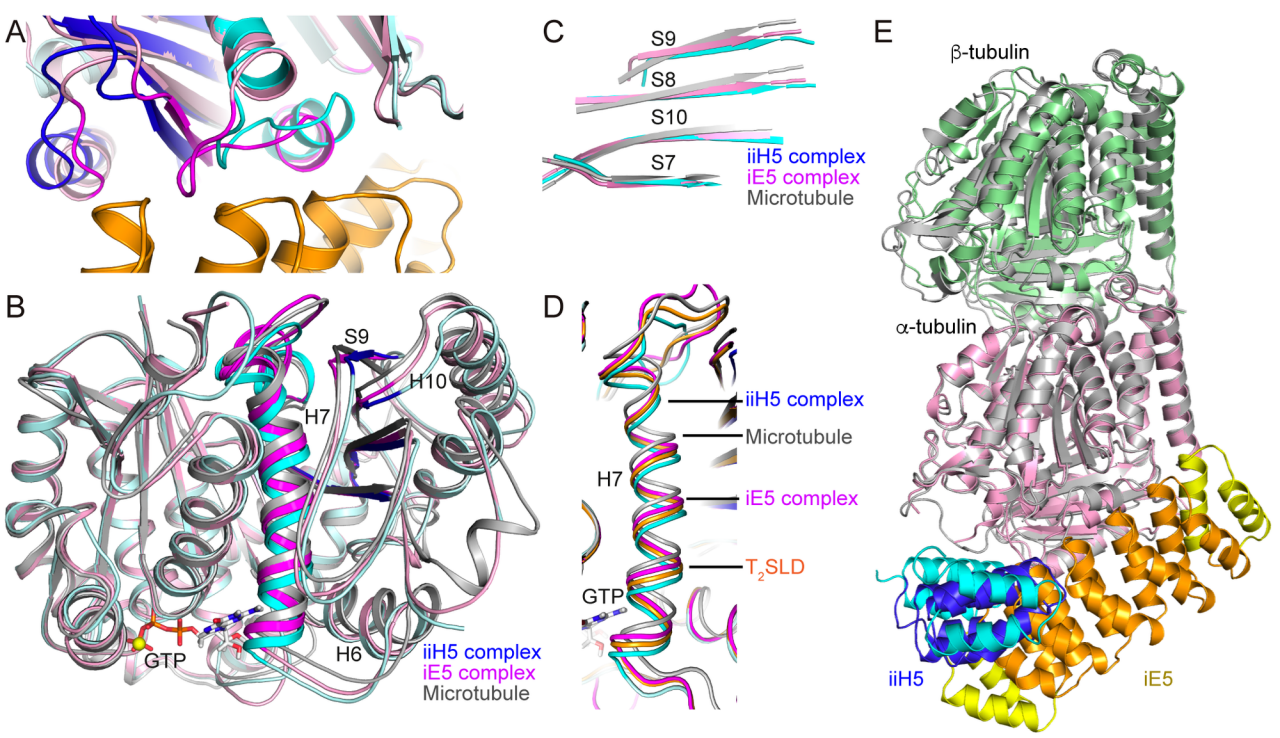
A
B
S9
H10
H7
GTP
H6
iiH5 complex
iE5 complex
Microtubule
C
S9
S8
S10
S7
iiH5 complex
iE5 complex
Microtubule
D
iiH5 complex
Microtubule
H7
iE5 complex
T2SLD
GTP
E
β-tubulin
α-tubulin
iiH5
iE5

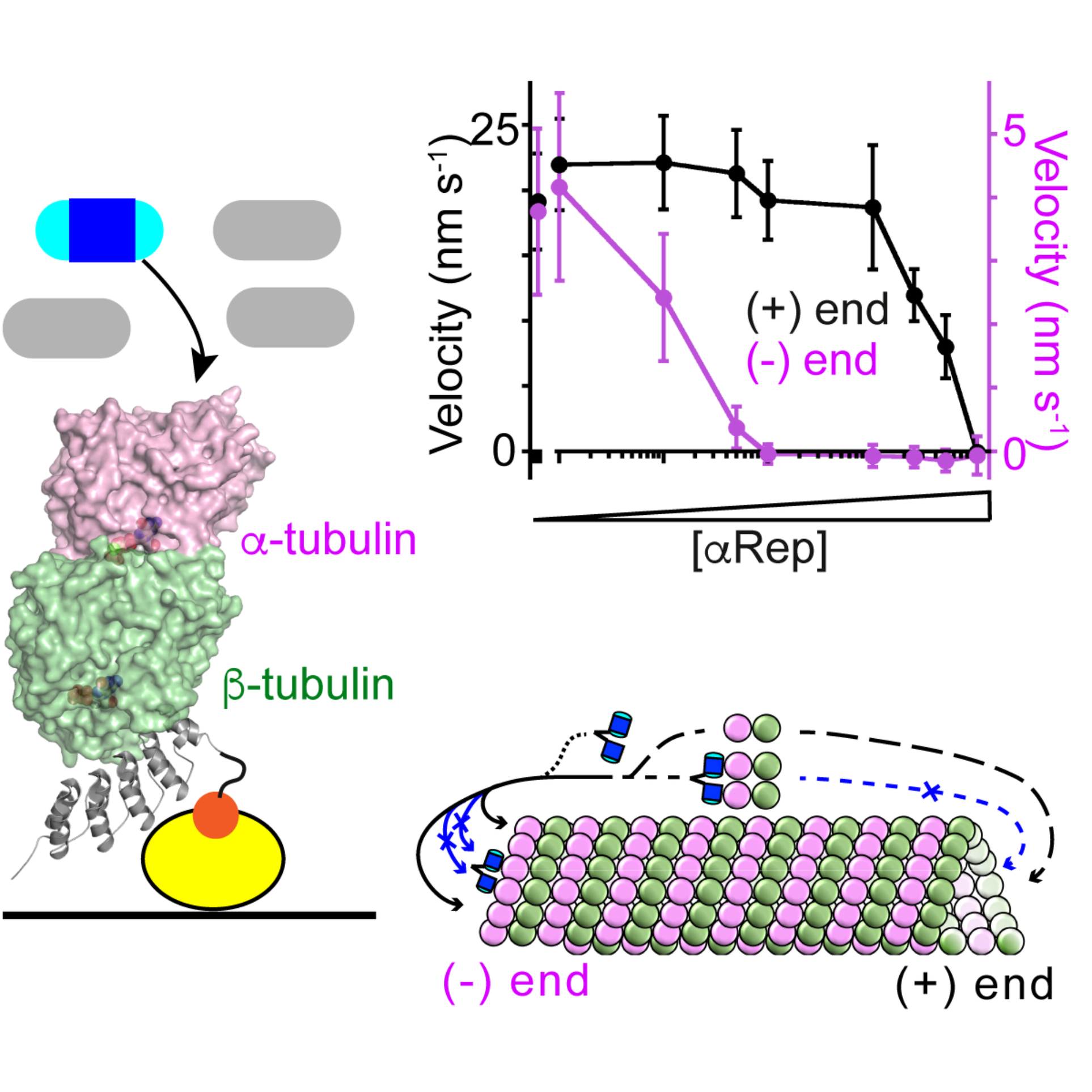
α-tubulin
β-tubulin
Velocity (nm s-1)
25
0
5
0
Velocity (nm s-1)
(+) end
(-) end
[αRep]
(-) end
(+) end